Letter

Cloud Effective Emissivity Retrievals Using Combined Ground-Based Infrared Cloud Measuring Instrument and Ceilometer Observations

Lei Liu [1],* , Ting Zhang [2], Yi Wu [3], Zhencong Niu [4] and Qi Wang [1]

[1] College of Meteorology and Oceanography, National University of Defense Technology,
    Nanjing 211101, China; qiqiqiwang@outlook.com
[2] Hebei Provincial Meteorological Bureau, CMA, Shijiazhuang 050000, China; stereo126@163.com
[3] Nanjing Meteorological Bureau, CMA, Nanjing 210019, China; yiwu_cma@outlook.com
[4] Army Aviation Institute, Beijing 101123, China; niuzhencong@163.com
* Correspondence: liuleidll@gmail.com; Tel.: +86-25-8083-0652

check for
updates

Abstract: In this paper, a new inversion procedure for cloud effective emissivity retrievals using a combined ground-based infrared cloud measuring instrument with ceilometer was developed. A quantitative sensitivity and performance analysis of the proposed method was also provided. It was found that the uncertainty of the derived effective emissivity was mainly associated with errors on the measurement radiance, the simulated radiance of clear sky and blackbody cloudy sky. Furthermore, the retrieval at low effective emissivity was most sensitive to the simulated clear sky radiances, whereas the blackbody cloudy sky radiance was the prevailing source of uncertainty at high emissivity. This newly proposed procedure was applied to the measurement taken in the CMA Beijing Observatory Station from November 2011 to June 2012 by the whole-sky infrared cloud-measuring system (WSIRCMS) and CYY-2B ceilometer. The cloud effective emissivity measurements were in good agreement with that of the MODIS/AQUA MYD06 Collection 6 (C6) cloud products. The mean difference between them was 0.03, with a linear correlation coefficient of 0.71. The results demonstrate that the retrieval method is robust and reliable.

Keywords: cloud effective emissivity; ground-based infrared cloud measuring instrument; ceilometer; joint observation; uncertainty analysis

1. Introduction

Clouds play a fundamental role in maintaining the Earth's energy balance. Although cloud properties such as cloud cover, cloud base height (CBH), and cloud type have been measured by human observers for a long time, there are still plenty of shortcomings. For instance, the measurements are subjective, inconsistent, and have a limited spatial density and temporal resolution. The research into developing a ground-based cloud measuring system has grown rapidly over recent years. Many instruments such as Total Sky Imager (TSI) [1], Whole Sky Imager (WSI) [2], Infrared Cloud Imager (ICI) [3], and whole-sky infrared cloud-measuring system (WSIRCMS) [4] have been developed and used for obtaining cloud properties in many countries.

The transition from humans to sensors for observing clouds would be a valuable achievement. In this process, the ground-based infrared cloud measuring systems have attracted much attention because they can be operated continuously during day and night with a constant sensitivity. Many efforts have been made to improve cloud detection, CBH determination, and cloud type classification using automatic IR cloud-measurements [5–7]. The performance of cloud cover measurement by these

IR cloud measuring systems is verified in [4,5,8]. CBH measurements by these instruments show reasonable agreement with ceilometers for only low-level cloud layers [5,9]. It is known that CBHs derived from the downwelling atmospheric infrared radiation based on the assumption that the cloud layers are blackbody. Low-level cloud layers are more likely to be thick and treated as a blackbody, while others are obviously not. Therefore, the difference in true-CBHs obtained by ceilometers and blackbody-like-CBHs from IR cloud measuring systems can be used to retrieve the cloud effective emissivity. Based on this principle, Garnier et al. [10] showed a satellite-based example for the purpose of retrieving high-level cloud effective emissivity using the combined dataset of the Imaging Infrared Radiometer (IIR) and Cloud–Aerosol Lidar and Infrared Pathfinder Satellite Observation (CALIPSO). Until now, only a few individual case studies related to the ground-based measured broadband infrared cloud emissivities could be found. Platt [11] used a radiometer and a Lidar to obtain the emissivity of high layer clouds. The sky radiance above the clouds was considered to be negligible because of the low water vapor content and low temperatures above high layer clouds [12]. This assumption is not suitable for other clouds, especially low-level and mid-level clouds. Shaw et al. [13] presented an approach to estimate the maximum probable cloud optical depth with a given value of observed radiance from ICI. However, Shaw's methodology requires a pre-estimation of the simulated cloud-radiances, cloud base heights, and optical depths measured by the Raman Lidar.

In this paper, we focused on the cloud effective emissivity estimation by using a combined ground-based infrared cloud imager and a ceilometer approach. The ceilometer was used to obtain the true CBH as the WMO considers that it is the most accurate and efficient tool for measuring cloud base from the ground when compared with alternative equipment [14]. The two instruments can both work continuously day and night, and have good complementarity. The novel method proposed in this paper will further obtain value-added cloud products in addition to cloud cover, cloud type, and cloud base height. The basics of the cloud effective emissivity retrieval algorithm that can be used for all types of cloud are presented in Section 2. Section 3 presents the sensitivity to the key parameters and associated uncertainties. Cases of inversion results and the statistical results of several months are shown and discussed in Section 4 before ending with the conclusions.

2. Instruments and Method

2.1. Specifications of the Instruments

The ground-based infrared cloud imager used in this paper was the WSIRCMS, which is a ground-based passive sensor that uses an uncooled microbolometer detector array to measure downwelling atmospheric radiance in the range of 8–14 μm wavelength bands [15]. It provides a way to obtain the cloud horizontal distributions, calculate the cloud cover, estimate the cloud base height, and classify the cloud type every 15 min with constant sensitivity during day and night. The primary WSIRCMS system contains an optical detector, environmental parameter sensors, controller, power and terminal unit, etc. The optical detector is an uncooled microbolometer array with 320×240 pixels. A whole sky image is obtained under the control of the scan servo system after combining the zenith image and other images at eight different orientations. The whole sky image has a resolution of 650×650 pixels. Given the calibration of the instrument in the laboratory [16], the uncertainty of the measured radiance was 0.72 W·m^{-2}·sr^{-1}. In the retrieval algorithm, clouds are treated as a blackbody when the CBH is derived from the downwelling infrared radiance. It is known that the blackbody assumption is not always valid, especially for mid-level and high-level clouds, so the retrieved CBH is not always the real height of the cloud base, and the former is usually called the equivalent CBH [9].

The ceilometer used in this study was a CYY-2B [17], produced by the CAMA (Luoyang) Environment Monitoring Limited Company. It is a biaxial ceilometer and emits laser pulses at 905 nm with a bandwidth <0.1 nm. The backscattered signal profiles typically have a vertical resolution of 5 m and a temporal resolution of 1 min. The instrument has a specified range of 10 km. To make the retrievals more credible, the CBHs derived from the CYY-2B ceilometer were reprocessed using the

temporal height tracking (THT) algorithm [18] in this paper. The THT algorithm uses the time-averaged backscatter maxima and backscatter gradient maxima to calculate the CBHs. An efficient filtering procedure of the spurious cloud bases as well as of the tracking system of each cloud layer was applied to avoid unrealistic jumps between two consecutive CBH determinations. Results showed that more accurate estimates of the CBH were obtained for simple and complex cloud patterns [18].

2.2. Principles of Cloud Effective Emissivity Retrieval

The downwelling radiation $R^\downarrow$ measured by WSIRCMS is related to the cloud and atmospheric radiative and thermodynamic properties by the relations as follows:

$$R^\downarrow = R_d + \varepsilon_c \tau_{p_c}^{p_s} B(T_c) + (1 - \varepsilon_c - r_c) \tau_{p_c}^{p_s} R_a + r_c \tau_{p_c}^{p_s} R_u \tag{1}$$

where R_d is the downwelling radiance from below the cloud to the surface; R_a is the downwelling radiance from above the cloud to the cloud top height; R_u is the upwelling radiance from below the cloud to the cloud base height; ε_c and r_c are the emissivity and the reflectivity of the cloud, respectively; B is the Planck function; T_c is the temperature of the cloud; p_c is the cloud base pressure; p_s is the surface pressure; and $\tau_{p_c}^{p_s}$ is the transmittance from p_c to p_s.

The emissivity of the cloud is then given by

$$\varepsilon_c = \frac{R^\downarrow - R_d - \tau_{p_c}^{p_s}(R_a + r_c R_u - r_c R_a)}{\tau_{p_c}^{p_s}(B(T_c) - R_a)} \tag{2}$$

The clear sky downwelling radiation can be expressed as

$$R_{clr}^\downarrow = R_a \tau_{p_c}^{p_s} + R_d \tag{3}$$

So,

$$\varepsilon_c = \frac{R^\downarrow - R_{clr}^\downarrow - r_c \tau_{p_c}^{p_s}(R_u - R_a)}{\tau_{p_c}^{p_s}(B(T_c) - R_a)} \tag{4}$$

If the cloud at the actual height Z_c that can be detected by the ceilometer is supposed to be a blackbody, ε_c is equal to 1. So that,

$$1 = \frac{R_{BB}^\downarrow - R_{clr}^\downarrow - r_c \tau_{p_c}^{p_s}(R_u - R_a)}{\tau_{p_c}^{p_s}(B(T_c) - R_a)} \tag{5}$$

According to Equations (4) and (5), the cloud emissivity can be calculated using Equation (6),

$$\varepsilon_c = \frac{R^\downarrow - R_{clr}^\downarrow - r_c \tau_{p_c}^{p_s}(R_u - R_a)}{R_{BB}^\downarrow - R_{clr}^\downarrow - r_c \tau_{p_c}^{p_s}(R_u - R_a)} \tag{6}$$

The cloud reflectivity term, which means the radiance reflected by the cloud from the surface and atmosphere under the cloud, is generally smaller than the cloud emission term by more than one order of magnitude. Yamamoto et al. [19] and Herman [20] indicated that the infrared broadband cloud reflectivity approached a maximum value of 0.03. Allen [21] pointed out that the error of the cloud emissivity caused by ignoring the reflectivity was of the order of 8%. This might be quite small, so, in this paper, the cloud reflectivity was set as zero [22]. The emissivity of the cloud is then given by Equation (7):

$$\varepsilon_{eff} = \frac{R^\downarrow - R_{clr}^\downarrow}{R_{BB}^\downarrow - R_{clr}^\downarrow} \tag{7}$$

From the above equations, we see that the cloud effective emissivity ε_{eff} can be calculated by the measured downwelling infrared radiation ($R^{\downarrow}$), the clear sky atmospheric downwelling radiation ($R^{\downarrow}_{clr}$), and the downwelling radiation of the blackbody clouds with known CBH ($R^{\downarrow}_{BB}$). The latter two should be obtained by the radiative transfer model. In this paper, we used the Santa Barbara Discrete Ordinate (DISORT) Atmospheric Radiative Transfer (SBDART) model [23] to perform the radiation simulations. The overall scheme of the method is described through the flow diagram shown in Figure 1. The dataset for the study was taken from the combined observations of the WSIRCMS and the CYY-2B ceilometer. The clear-sky radiance $R^{\downarrow}_{clr}$ can be calculated using vertical profiles of atmospheric pressure, temperature, and humidity measured by radiosondes. Since water vapor is the most important factor that affects the downwelling atmospheric radiance in the 8–14 μm wavelength bands [24], the gaps out of radiosonde time (performed operationally twice a day) were filled using the estimated precipitable water vapor. These values can be obtained using the real-time measurements of the surface temperature and humidity [4]. Assuming that the cloud radiates like a blackbody, the downwelling radiance for cloud layers ($R^{\downarrow}_{BB}$) at the heights of CBHs derived from the CYY-2B ceilometer can be also calculated by SBDART with a known atmospheric condition. Since the IR images of the zenith area observed by WSIRCMS every 15 min and the zenith viewing angle is about 60°, we took the intermediate value of the CBHs derived from the CYY-2B ceilometer during the WSIRCMS observation period. These CBHs were treated as the reference cloud base heights which were eventually put into the SBDART model.
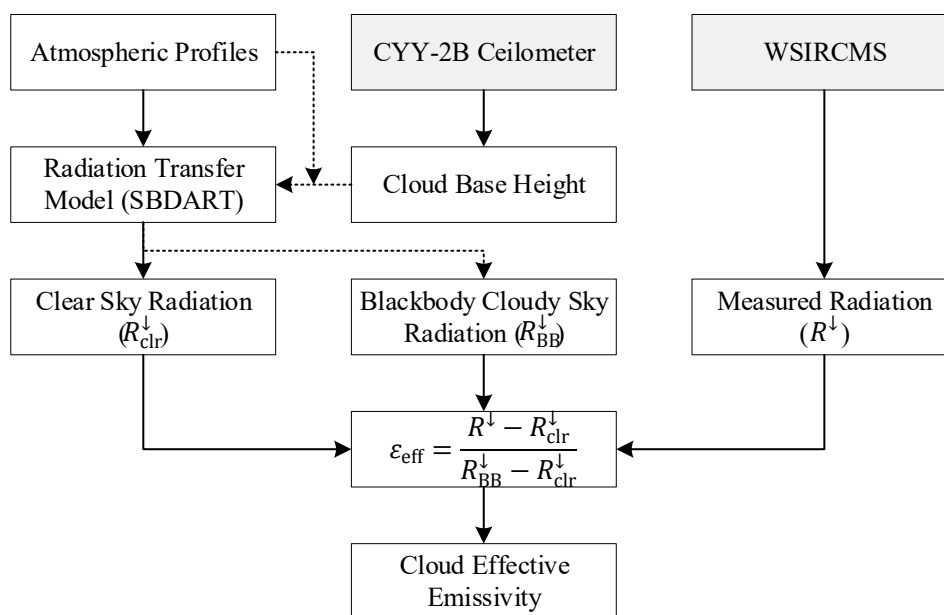

Figure 1. The cloud effective emissivity retrieval algorithm flow diagram.

3. Uncertainty Analysis of the Inverse Method

3.1. Uncertainty of Each Item Parameter

Inferred from Equation (7), the uncertainty of cloud effective emissivity mainly comes from the errors of the measured atmospheric downwelling infrared radiation $R^{\downarrow}$, the clear sky atmospheric downwelling radiation $R^{\downarrow}_{clr}$ obtained by the radiative transfer model, and the radiation $R^{\downarrow}_{BB}$ of the blackbody clouds with known base heights. The expressions of uncertainty in these three parts are as follows:

$$u_{\varepsilon_{eff},R^{\downarrow}} = \frac{\partial \varepsilon_{eff}}{\partial R^{\downarrow}} u_{R^{\downarrow}} = \frac{-1}{R^{\downarrow}_{clr} - R^{\downarrow}_{BB}} u_{R^{\downarrow}} \tag{8}$$

$$u_{\varepsilon_{eff},R_{clr}^{\downarrow}} = \frac{\partial \varepsilon_{eff}}{\partial R_{clr}^{\downarrow}} u_{R_{clr}^{\downarrow}} = \frac{\left(1 - \varepsilon_{eff}\right)}{R_{clr}^{\downarrow} - R_{BB}^{\downarrow}} u_{R_{clr}^{\downarrow}} \tag{9}$$

$$u_{\varepsilon_{eff},R_{BB}^{\downarrow}} = \frac{\partial \varepsilon_{eff}}{\partial R_{BB}^{\downarrow}} u_{R_{BB}^{\downarrow}} = \frac{\varepsilon_{eff}}{R_{clr}^{\downarrow} - R_{BB}^{\downarrow}} u_{R_{BB}^{\downarrow}} \tag{10}$$

It is shown that the effective emissivity uncertainty per radiance unit (a radiance unit (RU) is $1 \text{ W·m}^{-2}\text{·sr}^{-1}$) of the observed or simulated radiation error was related to the difference between the blackbody cloud radiation and the clear sky radiation, which is expressed as $R_{clr}^{\downarrow} - R_{BB}^{\downarrow}$. Generally, $R_{clr}^{\downarrow}$ is smaller than $R_{BB}^{\downarrow}$, so $R_{clr}^{\downarrow} - R_{BB}^{\downarrow}$ is less than zero. Figure 2 shows the effective emissivity uncertainty per RU of the radiance error versus the difference between the blackbody cloud radiation and the clear sky radiation, where Mea (solid lines) stands for the radiation measured by instrument. BG (dashed lines) is the clear sky radiation ($R_{clr}^{\downarrow}$) simulated by the model. BB (dotted lines) is the blackbody cloud radiation ($R_{BB}^{\downarrow}$) simulated by the model with measured CBH. Assuming that the difference between BB and BG ranges from -40 RU to -5 RU, the inversion errors of the cloud effective emissivities caused by observed or simulated radiation errors were computed for effective emissivities of 0.1 (triangle), 0.4 (cross), and 0.8 (square), respectively. It can be seen that all the effective emissivity uncertainties decreased with the increasing absolute values of $R_{clr}^{\downarrow} - R_{BB}^{\downarrow}$. The inversion uncertainty caused by clear sky radiation simulated errors increased with decreasing emissivities, whereas the effect of the blackbody cloud radiance uncertainty did the opposite. The inversion errors caused by measured radiance uncertainty did not change with the varied cloud emissivities.
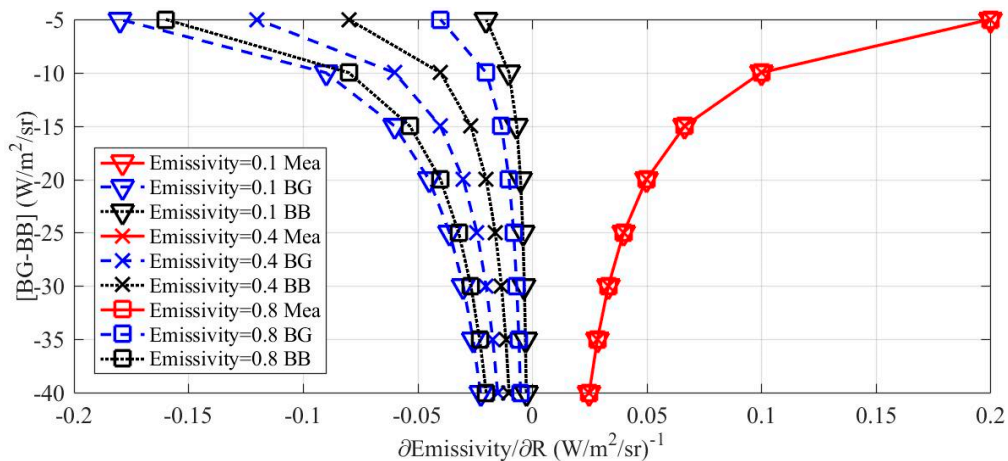

Figure 2. Effective emissivity uncertainty per radiance unit error on the measurement, the clear sky simulation, and the simulation of sky with blackbody cloud.

3.2. Overall Effective Emissivity Uncertainty Estimate

The overall effective emissivity uncertainty $u_{\varepsilon_{eff}}$ can be derived from the three independent contributions listed above.

$$\begin{aligned} u_{\varepsilon_{eff}} &= \sqrt{u_{\varepsilon_{eff},R^{\downarrow}}{}^2 + u_{\varepsilon_{eff},R_{clr}^{\downarrow}}{}^2 + u_{\varepsilon_{eff},R_{BB}^{\downarrow}}{}^2} = \\ &\frac{1}{\left| R_{clr}^{\downarrow} - R_{BB}^{\downarrow} \right|} \sqrt{u_{R^{\downarrow}}{}^2 + \left(1 - \varepsilon_{eff}\right)^2 u_{R_{clr}^{\downarrow}}{}^2 + \varepsilon_{eff}{}^2 u_{R_{BB}^{\downarrow}}{}^2} \end{aligned} \tag{11}$$

According to the previous research, given that the transmittance of the germanium glass protective window of WSIRCMS possibly decreases with the facility operation for a period of time, the uncertainty of measurement radiation ($u_{R\downarrow}$) was set as twice the calibration uncertainty with the value of 1.44 RU. Due to the error of input meteorological data to the model, the uncertainty of clear sky radiation ($u_{R_{clr}^{\downarrow}}$) calculated by the radiative transfer model was generally less than 5.0 RU in the zenith direction [25].

When blackbody clouds exist, the uncertainty of radiation calculated by the radiative transfer model is related to the error of the CBH. It can be calculated that the infrared radiation error caused by the 500 m cloud base height error of the blackbody cloud is about 1 RU [25].

The overall uncertainty under different cloud effective emissivities (0.1 (left panel), 0.4 (center panel), and 0.8 (right panel), respectively) is shown in Figure 3. Clear sky radiation errors of 1.0 RU, 3.0 RU, and 5.0 RU were considered. This shows that the error in the clear sky radiation was the prevailing source of uncertainty for low emissivity retrievals. For the cases where the difference between the clear sky radiation and the blackbody cloud was greater than 15 RU, the uncertainty associated with an effective emissivity of 0.1 was about 0.1 in the best conditions (1 RU clear sky radiation error), slightly degrading to a mean value of 0.2 for an error of 3 RU, and 0.3 for an error of 5 RU. The error in the blackbody cloud radiation was the prevailing source of uncertainty for high emissivity retrievals (right panel) with little impact from the clear sky radiation error.
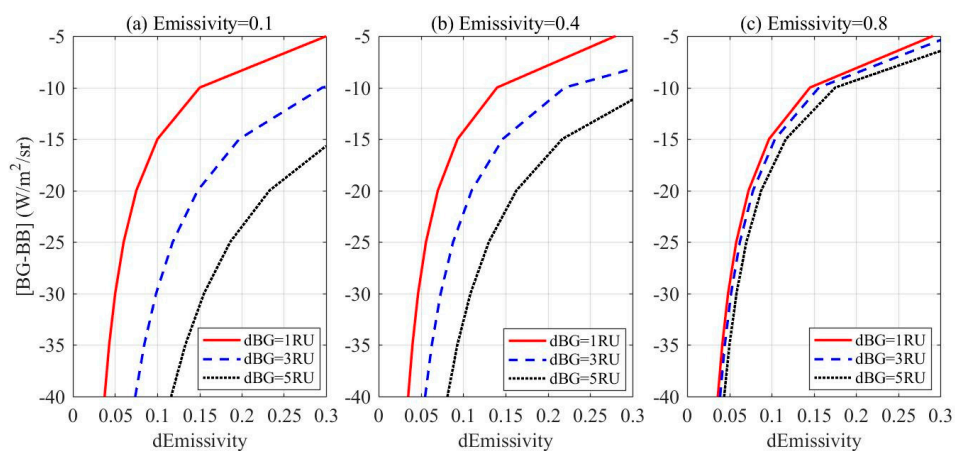

Figure 3. The overall uncertainty under different cloud effective emissivities.

4. Results and Discussions

To evaluate the performance of the retrieval algorithm, a series of cloud effective emissivity comparison experiments using the WSIRCMS and the CYY-2B ceilometer was performed at the Chinese Meteorological Administration (CMA) Beijing Observatory Station (39.813, 788°N, 116.480, 059°E, 55 m a.s.l.) from November 2011 to June 2012. Two cases are first discussed, then the retrieval results are validated with the recently released MODIS/AQUA MYD06 Collection 6 (C6) cloud products, which include the 8.5, 11, 12, and 13 μm cloud emissivity values. Finally, the average cloud emissivity for each cloud base height derived from the ground-based joint observation is shown and discussed. It should be noted that although this joint method can be used to estimate the cloud emissivity in the whole sky, the cloud emissivity described in this paper is only the inversion results in the zenith direction in order for a comparison with the satellite observations.

4.1. Cases Study

Figure 4 shows an example of the cloud effective emissivities of the zenith sky derived from the combined CYY-2B ceilometer and WSIRCMS on 29 November 2011. The reference CBHs derived from the CYY-2B ceilometer and the corresponding equivalent CBHs derived from the WSIRCMS are displayed in Figure 4a. It can be seen that from 04:00 to 16:00 local time (LT), the actual cloud base height of the low-level clouds observed on that day was almost the same as the equivalent cloud base height from the WSIRCMS. The cloud emissivities in this period were close to or equal to 1, which means that the cloud layers can be treated as a blackbody. This is the reason the true CBHs were equal to the equivalent CBHs. In other time periods, there were large differences between the reference CBHs and equivalent CBHs because those cloud layers were gray bodies. The emissivities of these mid-level and high-level cloud layers varied from 0.1 to 0.9 (Figure 4b). The four WSIRCMS zenith

images at the bottom of Figure 4 indicate the cloud distributions at 01:44, 08:44, 19:14, and 22:59 LT. Here, we found a good correspondence between the images and the emissivity results.
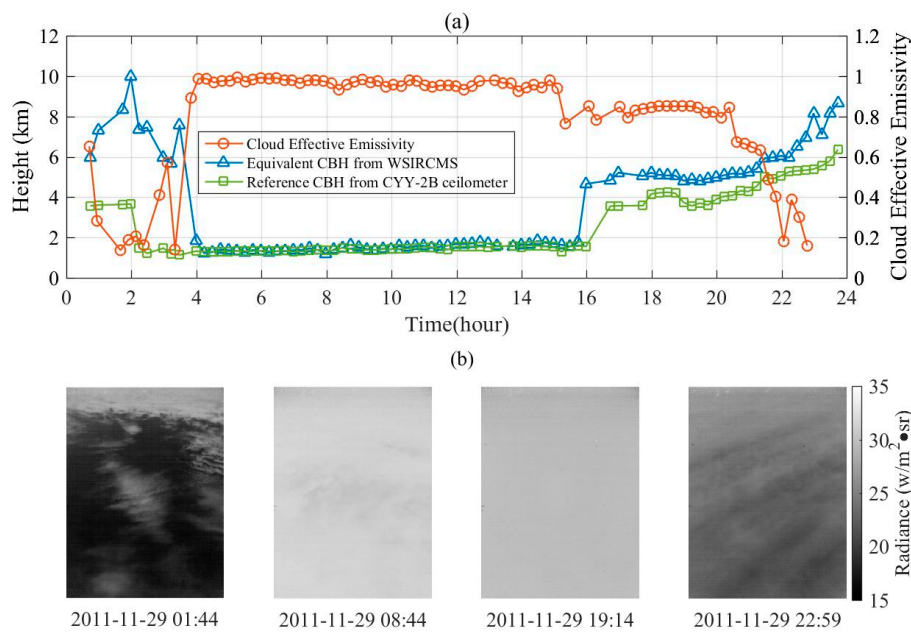

Figure 4. Example of the cloud effective emissivities derived from the joint observation (**a**) and corresponding images showing the zenith sky at 01:44, 08:44, 19:14, and 22:59 LT (from left to right) (**b**) at the CMA Beijing Observatory Station for 29 November 2011.

Another example of the low-level cloud layers on 2 March 2012 are shown in Figure 5. We can see that the reference CBHs showed few changes while the cloud effective emissivities varied significantly, especially after 12:00. The corresponding IR images in Figure 5b certify the fact that the actual clouds were not uniform. Low-level clouds cannot always be assumed to be a blackbody, which is the reason the derived IR effective cloud base height appears to be biased.
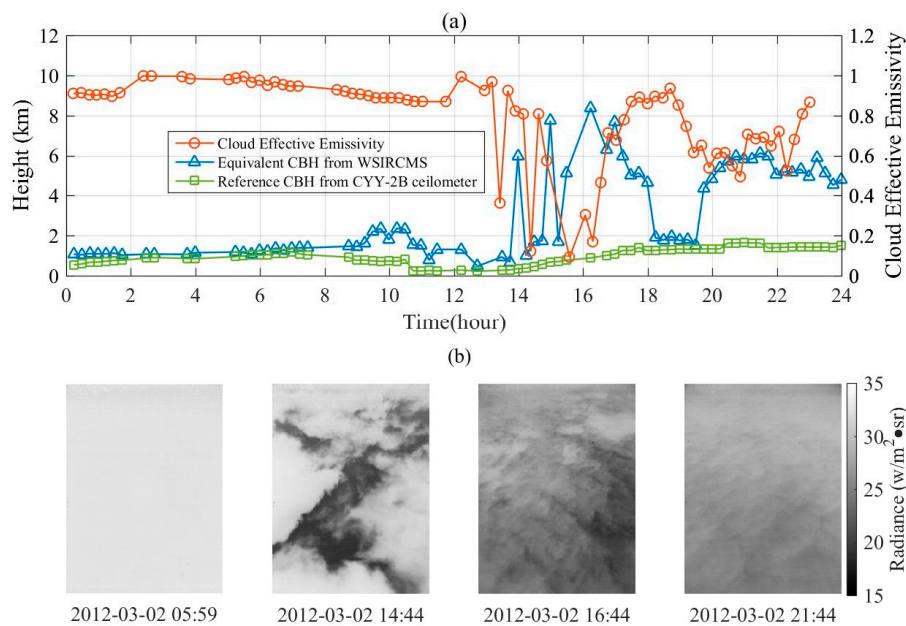

Figure 5. Example of cloud effective emissivities derived from the joint observation (**a**) and corresponding images showing the zenith sky at 05:59, 14:44, 16:44, and 21:44 LT (from left to right) (**b**) at the CMA Beijing Observatory Station for 2 March 2012.

4.2. Comparison with MODIS/AQUA MYD06 C6 Data

Figure 6 presents the cloud effective emissivities derived from the ground-based joint observation when compared with the MODIS/AQUA MYD06 C6 data for about seven months. The satellite passes over the CMA Beijing Observatory Station twice a day. A total of 417 MODIS observations during the test period were found. The recently released MYD06 Collection 6 (C6) cloud products include cloud emissivity values in four InfraRed (IR) channels located in the longwave IR-window (8.5, 11, 12, and 13 μm) [26]. In this paper, the cloud effective emissivity of each channel that was greater than 0 and less than or equal to 1.2 was taken as effective data. Thus, we obtained 183 sets for 8.5 μm, 180 sets for 11 μm, 184 sets for 12 μm, and 176 sets for 13 μm. In the corresponding period, the effective dataset of ground-based observations had 1382 groups. Finally, we plotted the probability histogram of these cloud effective emissivities in Figure 6. It can be seen that the ground-based observations were in good agreement with the MODIS/AQUA observations at 8.5, 11, and 13 μm. Both methods have the possibility of calculating emissivity greater than 1 which is due to the neglect of the reflection effect of clouds during both inversion methods, and the errors of the measurement and simulation process. In comparison, our method computed more clouds with an emissivity greater than 1 than the satellite observation method. At the same time, the rate of low cloud emissivity was also slightly higher. Nevertheless, when compared with the MODIS/AQUA observations, the method in this paper could produce reasonable cloud effective emissivity results.
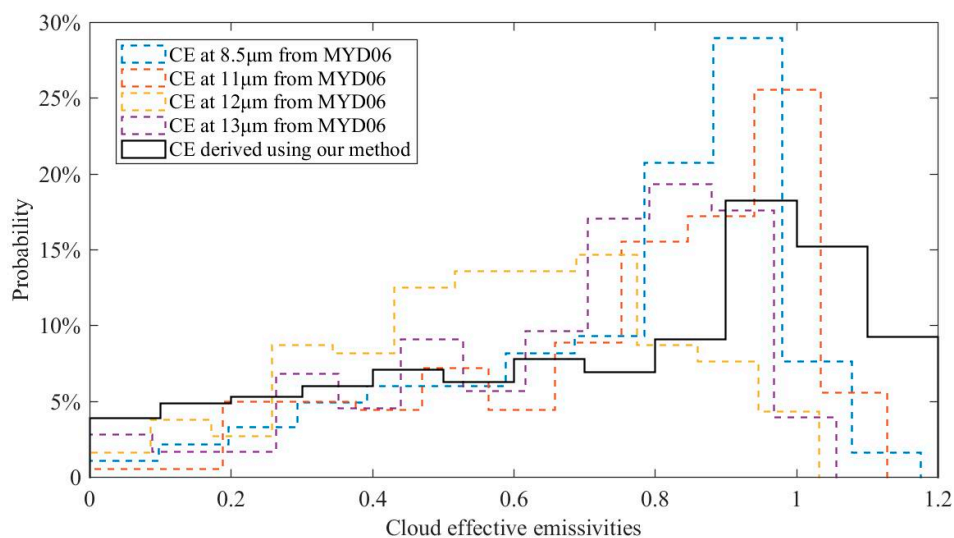

Figure 6. Histograms of cloud effective emissivities comparing the distribution from the derived from the MODIS/AQUA MYD06 C6 data and from the present data.

To investigate the relationship more deeply between the cloud effective emissivities derived from the ground-based observation and from the satellite-based datasets, we selected only data points that were within a 10 min time window centered around the MODIS/AQUA observations. We also required both observations to be less than 1.2 and greater than 0. This pre-conditioning, however, limited the comparison of our method with the MYD06 product to 22 data points at 8.5 μm, 20 data points at 11 μm, and 17 data points at 12 μm and 13 μm apart. Figure 7 shows a scatter plot of the effective data derived from the ground-based observations relative to the MYD06 product. A summary of the comparison of the cloud effective emissivities is presented in Table 1, where we show the bias, the bias standard deviation, the slope of a best-fit linear regression, and the linear correlation coefficient. Although the availability of the time-collocated datasets was very limited for comparison, some useful information could be inferred from them. This showed that the satellite- and ground-based retrievals were fairly well correlated with a linear correlation coefficient (r) of 0.71. The ground-based retrieval values were, on average, slightly higher than the MYD06 product with a mean difference of 0.03. As can

be seen in Table 1, there was a certain difference in the comparisons of the ground-based retrievals with MYD06 products at different wavenumbers. The ground-based retrievals compared better with the 8.5 μm MYD06 results than the others. The bias and the bias standard deviation between them was very small with an r of 0.75.

The difference between the two is mainly due to the difference in the observation angle and resolution. In addition, the retrieval algorithm and whether it is a multi-layer cloud are also related. Besides, both methods assume that the cloud is infinitely thin, while the actual cloud layer has a certain geometric height. The characteristics of cloud particles at the cloud top layers and bottom layers are different. For midlatitude cirrus clouds, it was observed that ice crystals in the top layers are normally small pristine particles with well-defined hexagonal structures, whereas ice crystals near the cloud base tend to be larger irregular particles [27,28]. The effect of this inhomogeneity can be quite significant for infrared channels for which ice is strongly absorptive. This is also an important reason for the difference.
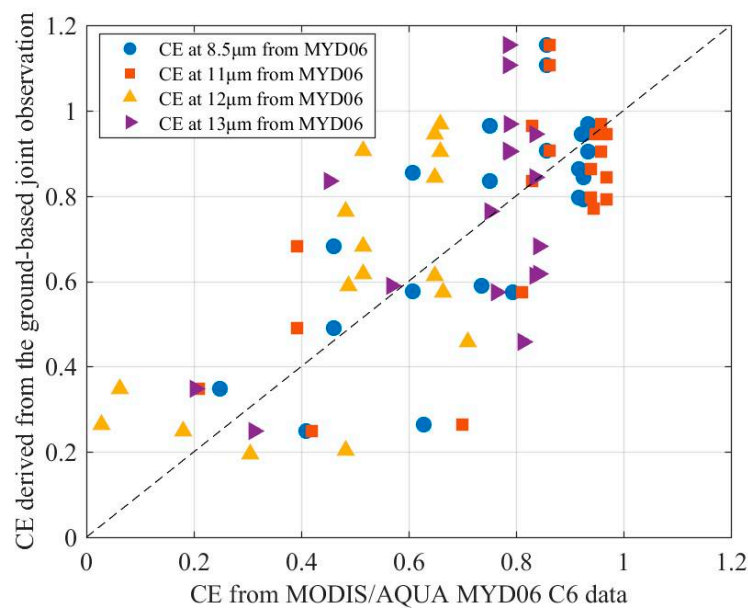

Figure 7. Difference between cloud effective emissivities observed by MODIS/AQUA and the ground-based joint instrument.

Table 1. Statistics of the comparison of the cloud effective emissivities shown in Figure 7: the mean bias, the std. dev. of the mean bias, the slope of a best-fit linear regression line, and the linear correlation coefficient values between the satellite- and ground-based retrievals.

Algorithm	No. of Samples	Mean Bias	Bias Std. Dev.	Slope	Linear Correlation Coef.
MYD06_8.5 μm	22	0.01	0.17	0.94	0.75
MYD06_11 μm	20	−0.02	0.19	0.80	0.73
MYD06_12 μm	17	0.11	0.20	0.85	0.68
MYD06_13 μm	17	0.03	0.22	0.72	0.56
All	76	0.03	0.19	0.78	0.71

4.3. Cloud Effective Emissivities for Different Cloud Base Height

The average cloud effective emissivity for each cloud base height derived from the joint observation is shown in Figure 8a. Overall, the cloud effective emissivity gradually decreased with the increase of the cloud base height. The average effective emissivity value of low-level cloud (from the Earth's surface to 2.5 km) was 0.95, the mid-level cloud (2.5 to 6 km) was 0.57, while the high-level cloud (above 6 km) was 0.33. In addition, the histogram of cloud emissivity corresponding to the low-level, mid-level, and high-level cloud are given in Figure 8b. The low-level cloud emissivity tended to be above 0.8, but clouds with low emissivity also exist. The emissivity of the mid-level cloud

was relatively evenly distributed over the range of 0 to 1 while that of the high-level cloud was mainly distributed below 0.7.
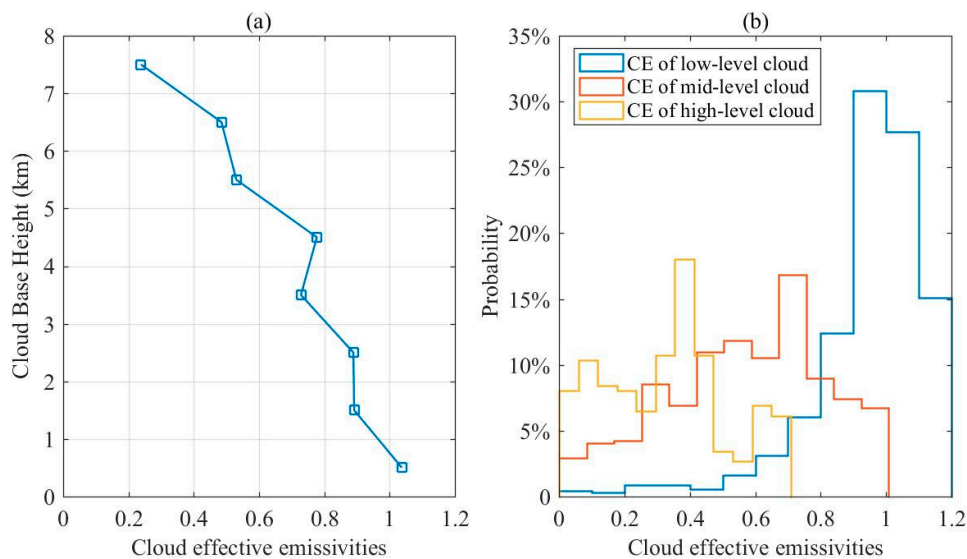

Figure 8. Cloud effective emissivities for different cloud base heights. (**a**) the average cloud effective emissivities for cloud layers at different height (0–1 km, 1–2 km, 2–3 km, 3–4 km, 4–5 km, 5–6 km, 7–8 km); (**b**) histograms of effective emissivities for low-level, mid-level, and high-level clouds.

5. Conclusions

A novel methodology for the retrieval of broadband longwave cloud effective emissivity was discussed in this paper. A ground-based infrared cloud measuring instrument combined with a laser ceilometer was utilized in the present study. Sensitivity analysis showed that the uncertainty of the derived effective emissivity was mainly associated with the errors of the measurement radiance, the simulated radiance of clear sky and blackbody cloudy sky. The retrieval of low effective emissivity was mostly sensitive to the simulated clear sky radiances whereas the blackbody cloudy sky radiance was the major source of uncertainty at high emissivity. An experiment was conducted at the CMA Beijing Observatory Station. The results of the present measurements were in good agreement with those of the MODIS/AQUA MYD06 Collection 6 (C6) cloud products. Statistical analysis was carried out for cloud effective emissivities at different cloud base heights. Due to the ignorance of the reflection effect of clouds in the inversion process, the derived cloud emissivities may be higher than 1. Reasonable amendments to data may overcome this problem and will be verified in the next stage of research. In addition, more complete validation with an extended dataset will be undertaken. Cloud emissivities for different cloud types can also be statistically analyzed in future study.

Author Contributions: Data curation, L.L., T.Z. and Z.N.; Formal analysis, L.L. and Y.W.; Funding acquisition, L.L.; Investigation, L.L. and Y.W.; Methodology, L.L., T.Z. and Y.W.; Validation, L.L., Z.N., and Q.W.; Visualization, T.Z., Z.N. and Q.W.; Writing—original draft, L.L. and T.Z.; Writing—review & editing, L.L., T.Z. and Q.W.

Conflicts of Interest: The authors declare no conflict of interest.

References

1.　Long, C.N.; Sabburg, J.M.; Calbó, J.; Pagès, D. Retrieving cloud characteristics from ground-based daytime color all-sky images. *J. Atmos. Ocean. Technol.* **2006**, *23*, 633–652. [CrossRef]

2.　Shields, J.E.; Karr, M.E.; Johnson, R.W.; Burden, A.R. Day/night whole sky imagers for 24-h cloud and sky assessment: History and overview. *Appl. Opt.* **2013**, *52*, 1605–1616. [CrossRef] [PubMed]

3.　Shaw, J.A.; Nugent, P.W. Physics principles in radiometric infrared imaging of clouds in the atmosphere. *Eur. J. Phys.* **2013**, *34*, 111–121. [CrossRef]

4.　Liu, L.; Sun, X.-J.; Gao, T.-C.; Zhao, S.-J. Comparison of cloud properties from ground-based infrared cloud measurement and visual observations. *J. Atmos. Ocean. Technol.* **2013**, *30*, 1171–1179. [CrossRef]

5.　Feister, U.; Möller, H.; Sattler, T.; Shields, J.; Görsdorf, U.; Güldner, J. Comparison of macroscopic cloud data from ground-based measurements using VIS/NIR and IR instruments at Lindenberg, Germany. *Atmos. Res.* **2010**, *96*, 395–407. [CrossRef]

6.　Nugent, P.W.; Shaw, J.A.; Pust, N.J. Correcting for focal-plane-array temperature dependence in microbolometer infrared cameras lacking thermal stabilization. *Opt. Eng.* **2013**, *52*, 061304. [CrossRef]

7.　Liu, L.; Sun, X.; Chen, F.; Zhao, S.; Gao, T. Cloud classification based on structure features of infrared images. *J. Atmos. Ocean. Technol.* **2011**, *28*, 410–417. [CrossRef]

8.　Boers, R.; de Haij, M.J.; Wauben, W.M.F.; Baltink, H.K.; van Ulft, L.H.; Savenije, M.; Long, C.N. Optimized fractional cloudiness determination from five ground-based remote sensing techniques. *J. Geophys. Res. Atmos.* **2010**, *115*. [CrossRef]

9.　Liu, L.; Sun, X.-J.; Liu, X.-C.; Gao, T.-C.; Zhao, S.-J. Comparison of cloud base height derived from a ground-based infrared cloud measurement and two ceilometers. *Adv. Meteorol.* **2015**, *2015*, 1–8. [CrossRef]

10.　Garnier, A.; Pelon, J.; Dubuisson, P.; Faivre, M.; Chomette, O.; Pascal, N.; Kratz, D.P. Retrieval of cloud properties using CALIPSO Imaging Infrared Radiometer. Part I: Effective Emissivity and Optical Depth. *J. Appl. Meteorol. Climatol.* **2012**, *51*, 1407–1425. [CrossRef]

11.　Platt, C.M.R. Remote Sounding of High Clouds: I. Calculation of visible and infrared optical properties from lidar and radiometer measurements. *J. Appl. Meteorol.* **1979**, *18*, 1130–1143. [CrossRef]

12.　Platt, C.M.R.; Dilley, A.C. Remote sounding of high clouds: II. Emissivity of cirrostratus. *J. Appl. Meteorol.* **1979**, *18*, 1144–1150. [CrossRef]

13.　Shaw, J.A.; Nugenta, P.W.; Pusta, N.J.; Redmana, B.J.; Piazzollab, S. Cloud optical depth measured with ground-based, uncooled infrared imagers. *Proc. SPIE* **2012**, *8523*, 85231D.

14.　Costa-Surós, M.; Calbó, J.; González, J.A.; Martin-Vide, J. Behavior of cloud base height from ceilometer measurements. *Atmos. Res.* **2013**, *127*, 64–76. [CrossRef]

15.　Sun, X.; Liu, L.; Zhao, S. Whole sky infrared remote sensing of cloud. *Procedia Earth Planet. Sci.* **2011**, *2*, 278–283. [CrossRef]

16.　Xuejin, S.; Jian, L.; Shijun, Z.; Dongli, Z.; Jietai, M. Radiometric Calibration Model of Uncooled Infrared Focal Plane Array. *J. PLA Univ. Sci. Technol.* **2008**, *9*, 399–403.

17.　Liu, L.; Zhang, T.; Wu, Y.; Wang, Q.; Gao, T. Accuracy analysis of the aerosol backscatter coefficient profiles derived from the CYY-2B ceilometer. *Adv. Meteorol.* **2018**. [CrossRef]

18.　Martucci, G.; Milroy, C.; O'Dowd, C.D. Detection of cloud-base height using Jenoptik CHM15K and Vaisala CL31 Ceilometers. *J. Atmos. Ocean. Technol.* **2010**, *27*, 305–318. [CrossRef]

19.　Yamamoto, G.; Tanaka, M.; Asano, S. Radiative transfer in water clouds in the infrared region. *J. Atmos. Sci.* **1970**, *27*, 282–292. [CrossRef]

20.　Herman, G.F. Thermal radiation in Arctic stratus clouds. *Q. J. R. Meteorol. Soc.* **1980**, *106*, 771–780. [CrossRef]

21.　Allen, J.R. Measurements of cloud emissivity in the 8–13 μ waveband. *J. Appl. Meteorol.* **1971**, *10*, 260–265. [CrossRef]

22.　DeSlover, D.H.; Smith, W.L.; Piironen, P.K.; Eloranta, E.W. A methodology for measuring cirrus cloud visible-to-infrared spectral optical depth ratios. *J. Atmos. Ocean. Technol.* **1999**, *16*, 251–262. [CrossRef]

23.　Ricchiazzi, P.; Yang, S.; Gautier, C.; Sowle, D. SBDART: A research and teaching software tool for plane-parallel radiative transfer in the earth's atmosphere. *Bull. Am. Meteorol. Soc.* **1998**, *79*, 2101–2114. [CrossRef]

24.　Zhang, T.; Wen, J.; Velde, R.v.d.; Meng, X.; Li, Z.; Liu, Y.; Liu, R. Estimation of the total atmospheric water vapor content and land surface temperature based on aatsr thermal data. *Sensors* **2008**, *8*, 1832–1845. [CrossRef] [PubMed]

25.　Liu, L. *Retrievals of Cloud Macro- and Micro-physical Properties Using Ground-Based Infrared Remote Sensing Method*; PLA University of Science and Technology: Nanjing, China, 2015.

26. Heidinger, A.; Li, Y.; Baum, B.; Holz, R.; Platnick, S.; Yang, P. Retrieval of cirrus cloud optical depth under day and night conditions from MODIS collection 6 cloud property data. *Remote Sens.* **2015**, *7*, 7257–7271. [CrossRef]

27. Heymsfielda, A.J.; Lewisa, S.; Bansemera, A.; Iaquintaa, J.; Miloshevicha, L.M.; Kajikawab, M.; Twohyc, C.; Poellotd, M.R. A general approach for deriving the properties of cirrus and stratiform ice cloud particles. *J. Atmos. Sci.* **2002**, *59*, 3–29. [CrossRef]

28. Mace, G.G.; Zhang, Y.; Platnick, S.; King, M.D.; Minnis, P.; Yang, P. Evaluation of cirrus cloud properties derived from MODIS data using cloud properties derived from ground-based observations collected at the ARM SGP site. *J. Appl. Meteorol.* **2005**, *44*, 221–240. [CrossRef]